

The sensitivity of the heat exchange at sea surface to meso and sub-basin scale eddies Model study for the Black Sea

Emil V. Stanev^{*,1}, Joanna V. Staneva²

Department of Meteorology and Geophysics, University of Sofia, 5 James Bourchier street, 1126 Sofia, Bulgaria

Accepted 17 July 2000

Abstract

The heat exchange between the atmosphere and ocean (a function of the difference between the sea surface temperature and atmospheric temperature) is differently accounted for in numerical models, depending on their horizontal resolution. This could result in large differences in the rates of formation of water masses in coarse resolution and eddy resolving models. We address this issue in the present paper comparing simulations carried out with the modular ocean model (MOM), which is set-up with coarse ($1/4^\circ$) and eddy ($1/12^\circ$) resolution. Both models are forced by atmospheric analysis data. The Black Sea is used as a test area, since it has well constrained heat balance. The absence of large open boundaries, which is not usually the case in most ocean models, precludes the dependency of the results on poorly known open boundary conditions and makes possible to accurately evaluate the model heat fluxes associated with mesoscale processes. We find many indications that the transport and mixing associated with mesoscale eddies provide an important mechanism for the penetration of cold surface water into the pycnocline. Their contribution is illustrated on the example of heat exchange with the atmosphere and the resulting intermediate water mass formation. Two areas are investigated in more detail: the shelf edge/continental slope area, where the time averaged patterns of cooling are realistically simulated in eddy resolving models, and the area of anticyclonic circulation between the coast and the main current the latter following approximately the continental slope. It is shown that the winter convection is enhanced at the periphery of coastal anticyclones. Lateral intrusions of coastal waters into the pycnocline associated with eddies govern the characteristics of cold intermediate water and the amplitude of annual signal at these depths. Statistical characteristics quantifying the contribution of mean versus

*Corresponding author. Tel.: +359-2-6256-289; fax: +359-2-9625-276.

E-mail address: stanev@phys.uni-sofia.bg (E.V. Stanev).

¹Current affiliation: ICBM, University of Oldenburg, Germany.

²Current affiliation: National Institute of Meteorology and Hydrology, Bulgarian Academy of Science, Sofia, Bulgaria.

eddy part of the heat flux at sea surface in the two models are analyzed. © 2001 Elsevier Science B.V. All rights reserved.

Keywords: Heat exchange; Mesoscale eddies; Watermass formation; Black sea

1. Introduction

One of the first issues addressed after the eddy-resolving ocean models became available was about the impact of the horizontal resolution on the meridional overturning. The studies of Cox (1985) and Bryan (1986) showed that eddies do not significantly affect the meridional heat transport. The sensitivity of eddy-resolving model to surface thermal boundary conditions was recently re-examined by Xu et al. (1995). They proved that the ocean response was very sensitive to the way how the atmosphere was represented: with zero heat capacity, with an infinite heat capacity, or as responding (even in a simple way) to the anomalies in the sea surface temperature (SST). An important point, here, is that the heat exchange is a function of the difference between the SST and the atmospheric temperature, thus, the correlation between the two fields simulated under different resolutions could differ, resulting in different estimates for the heat flux.

In the present study, we analyze the water mass formation and its relationship to the heat flux at sea surface as dependent on ocean eddies. This is a fundamental issue in the ocean-atmosphere exchange which has been disregarded in the ocean modeling. We use the Black Sea as a test area. This landlocked sea (Fig. 1) presents a useful test case for studies of the water mass formation in basins of estuarine type. The balance between the freshwater flux at the sea surface and the exchange in the Straits of Bosphorus controls the depth of the halocline which is the main thermohaline characteristic. The heat balance is well constrained with a net value much smaller than the local/instantaneous values (Staneva

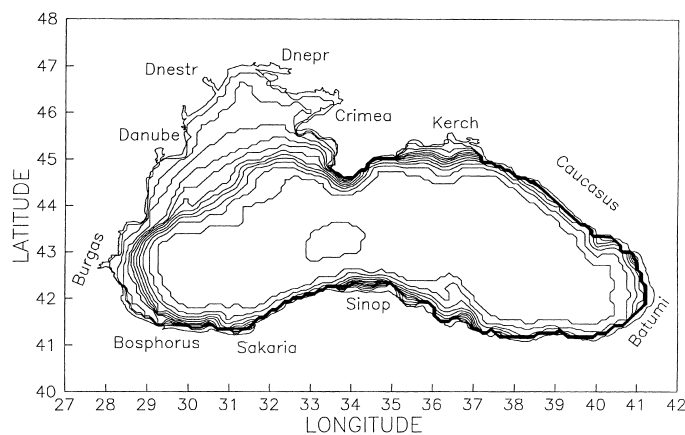


Fig. 1. Model topography. Isolines are plotted at 12 model levels: 7.5, 17.5, 35, 55, 75, 105, 185, 310, 515, 870, 1470, and 2125 m.

et al., 1995). Another important thermohaline feature is the cold intermediate layer (CIL). This thin and shallow (between 40–120 m) layer reveals how weak the ventilation in the stagnant basins is. The major factor controlling the characteristics of cold intermediate water (CIW) is the dependency of convection and mixing on the vertical stratification. In the Black Sea, the winter convection terminates at very shallow depths, and the small turbulent mixing in the seasonal thermocline tends to reduce in summer the heat flux from above. Thus, the cold water remains sandwiched between surface and deep layers as in a thermostat (for more details on this fundamental mechanism of water mass formation in the Black Sea, see Friedrich and Stanev, 1988; Stanev, 1988, 1990). The above considerations are reminiscent of the analogous process governing the formation of mode waters in the Atlantic Ocean.

The existing ideas about the formation of CIW are based on the analysis of survey data, taken usually in limited regions or for relatively short time. It is not easy to identify from such data the areas favoring the CIW formation. Even more difficult is to determine the local characteristics of convection. This motivated the use of numerical simulations that facilitate the understanding of water mass formation in the Black Sea (Stanev, 1988, 1990). The response of the CIL to variability in the atmospheric forcing was later analyzed by Stanev et al. (1995) and Oguz and Malanotte-Rizzoli (1996). Most of the earlier modeling studies did not address the impact of eddies on water mass formation, though the horizontal discretization in some of them (Oguz and Malanotte-Rizzoli, 1996; Rachev and Stanev, 1997) provided eddy resolution. The recent modeling study of Staneva and Stanev (1997) was devoted to this problem and made possible to explain the major mechanisms controlling the penetration of the CIW into the halocline.

The high frequency oscillations in the atmosphere trigger ocean convection, thus, smoothing of the meteorological data reduces the effectiveness of convection events in the ocean models. Without these events, the efficiency of cooling is underestimated. Forcing the ocean models with monthly averaged data, interpolated to model time steps could then result in substantial reduction of the heat exchange between the atmosphere and ocean (Hasselmann, 1976; Willebrand, 1978; Large et al., 1991). This could change the rates of formation of water masses and, as it has been shown on the example of Black Sea (Stanev et al., 1995), induce climatic changes with time scales much longer than those of convection. The impact of spatial averaging on the estimates of heat flux between atmosphere and ocean appears to be much more connected with the integral statistical characteristics than with the mean meteorological parameters (Gulev, 1994). As it was shown in this study the effect of spatial averaging on scales of >200 km is comparable to the effect of temporal averaging of 8–12 days. Unlike to our earlier work, dedicated to processes with small time scales (Stanev et al., 1995), we analyze, here, the water mass formation, focusing on small length scales. Additional motivations for the present study are given by the sensitivity analysis of Staneva et al. (1995), where it was shown that neglecting the correlation structure in space between meteorological data and SST drastically affects the heat flux estimates.

We analyze in this paper the sensitivity of the oceanic response to horizontal resolution of numerical model, keeping atmospheric data identical in all experiments. We will demonstrate that the discussion in the Black Sea oceanography about the relative importance of different mechanisms contributing to the CIW formation could be regarded as particular case of the more general issue being to what extent the interaction of atmosphere and ocean in this region is dominated by eddies. In contrast to the previous study of Staneva and Stanev

(1997), we do not investigate here the model performance with respect to formation and propagation of CIW, but rather the heat fluxes, associated with the mesoscale processes.

The paper is organized as follows: description of the model, model circulation and preconditioning of convection, heat exchange with the atmosphere, and final discussion and conclusions.

2. Model description

This study employs Pacanowski et al. (1991) modular ocean model (MOM), based on the work of Bryan (1969). Solid boundaries are non-slip and insulating for temperature and salinity. The model assumes the following boundary conditions at sea surface ($z = 0$):

$$w = 0, \rho_0 A_v \mathbf{U}_{hz} = \vec{\tau} \quad (1)$$

$$\rho_0 C_p K_v T_z = Q^T, \quad K_v S_z = \eta(S^* - S)\Delta z \quad (2)$$

where $\vec{\tau}$ is the wind stress, Q^T the surface heat flux, S^* the climatological salinity, η an inverse time scale and Δz the thickness of the first model layer (for other notations see Appendix A and B). Convection is parameterized by convective adjustment that is often used to remove static instabilities. Different implementations of this scheme exist starting from the original scheme of Bryan (1969) comparing the density in the adjacent layers and mixing temperature and salinity in unstable cases, the scheme of Marotzke (1991) mixing the whole unstable column, and the recent approach of Klinger et al. (1996) introducing finite adjustment time scales. Having in mind that the convection in the Black Sea reaches very shallow depths (50–70 m), which is a consequence of the extremely strong stratification, we could expect that instantaneous mixing in the vertical is appropriate for the representation of the process removing the instability. Even in the ocean case, the simplest (instantaneous) schemes are correct as it has been proved by Klinger et al. (1996). The above considerations justify using in the model the original scheme of Bryan. The number of convective loops has been made consistent with the model resolution to produce efficient removal of instabilities. The parameterizations of the surface forcing and subgrid processes are described in Appendix A and B.

We set-up two models with different resolutions. The first model has relatively coarse horizontal resolution of $1/4^\circ$ in latitude and $1/3^\circ$ in longitude (almost square grid elements of 28 km). In the second one, we increase the resolution three times ($1/12^\circ$ in latitude and $1/9^\circ$ in longitude). Both models have 24 vertical levels, with model depths at 2.5, 7.5, 12.5, 17.5, 25, 35, 45, 55, 65, 75, 85, 105, 140, 185, 240, 310, 400, 515, 665, 870, 1145, 1470, 1820, and 2125 m. Bottom topography (Fig. 1) is taken from the UNESCO bathymetric map and discretized with the model resolution.

The atmospheric forcing is prepared by adding high frequency signal from twice daily atmospheric analysis data for temperature, relative humidity and winds at sea surface (produced in the US National Meteorological Center, (NMC)) to the climatic data of Sorkina (1974). Our previous analysis (Staneva and Stanev, 1997; Stanev et al., 1997) demonstrates that such data set provides both correct climate and high frequency oscillations. This gives adequate signals needed for the water mass formation. Since the model heat flux depends on the simulated SST (see Eqs. (A.1) and (A.2)), we expect that the different correlation

structure between the SST and atmospheric variables, simulated under different resolution, will dominate the model heat balance. Here, we stress that identical atmospheric data are interpolated in the grid points of the two models, but each model produces its own fluxes at the sea surface which is dependent on the current SST.

Sea surface salinity is relaxed to time variable climatological data, interpolated linearly at every model time step from monthly mean data. The salt balance in the model is closed at the Straits of Bosphorus by continuously adding positive salinity flux. This flux is calculated from the diagnosed salinity flux at sea surface using a simple physical model for the water exchange in the strait. Details for the motivation of this approach, its relevance to the Black Sea conditions, and its implementation are given in the works of Stanev et al. (1997) and Staneva and Stanev (1998).

The coarse resolution model (CRM) is integrated for 20 years until an almost periodic solution is reached. Then the fine resolution model (FRM) is initialized with the data simulated in the CRM, and the two models are further integrated for 6 years (beginning from 1 January 1980). Though the analysis of the simulations show stable behavior of model statistics (including vertical stratification) the results are subject to some caveats since the period of integration is not sufficient to reaching complete statistical equilibrium.

Most of the results below, and particularly the ones from the intercomparisons between CRM and FRM are shown for 1986. More detailed analysis on the model behavior, including basin mode oscillations, baroclinic instabilities and eddy formation can be found in the paper by Rachev and Stanev (1997). The performance of the two models in simulating the water mass formation is discussed in the papers by Stanev et al. (1997) and Staneva and Stanev (1997).

3. Model circulation and preconditioning for convection

The main driving forces in the Black Sea are characterized by positive wind stress curl and negative flux of buoyancy caused by the fresh water flux (Stanev, 1990; Staneva and Stanev, 1998). A positive haline buoyancy flux in the Strait of Bosphorus compensates the surface buoyancy flux. The haline buoyancy flux at sea surface $B_S = g\beta Q_f S/A$ ($Q_f = 10^4 \text{ m}^3 \text{ s}^{-1}$ is the fresh water flux, Unluata et al., 1990, $S = 18 \text{ psu}$, $\beta = 0.78 \times 10^{-3} \text{ psu}^{-1}$ is the coefficient of haline contraction, and $A = 4.12 \times 10^5 \text{ km}^2$ is the surface area) is $-3.4 \times 10^{-9} \text{ m}^2 \text{ s}^{-3}$. The thermal buoyancy flux at sea surface $B_H = \alpha g F_H / (\rho_0 C_p)$ is smaller. If we take for the net cooling in 1986 $F_H = -1.7 \text{ W m}^{-2}$ (see further in text) and for the coefficient of thermal expansion $\alpha = 0.13 \times 10^{-3} \text{ K}^{-1}$, we obtain $B_H = 0.482 \times 10^{-9} \text{ m}^2 \text{ s}^{-3}$. If we calculate the buoyancy flux taking the winter mean value for heat flux $F_H = -200 \text{ W m}^{-2}$, we obtain $B_H = 47.058 \times 10^{-9} \text{ m}^2 \text{ s}^{-3}$, which demonstrates that the cooling dominates the buoyancy flux in winter. Thus, we could expect that cooling and the resulting convection would govern the thermodynamics of the Black Sea model in winter.

In order to illustrate the dynamics in CRM and FRM which preconditions the winter convection, we analyze below the model circulation, temperature and salinity fields. The annual mean total transport stream function (Fig. 2) is cyclonic during the whole year and shows one gyre system (rim current). This type of circulation was confirmed many times

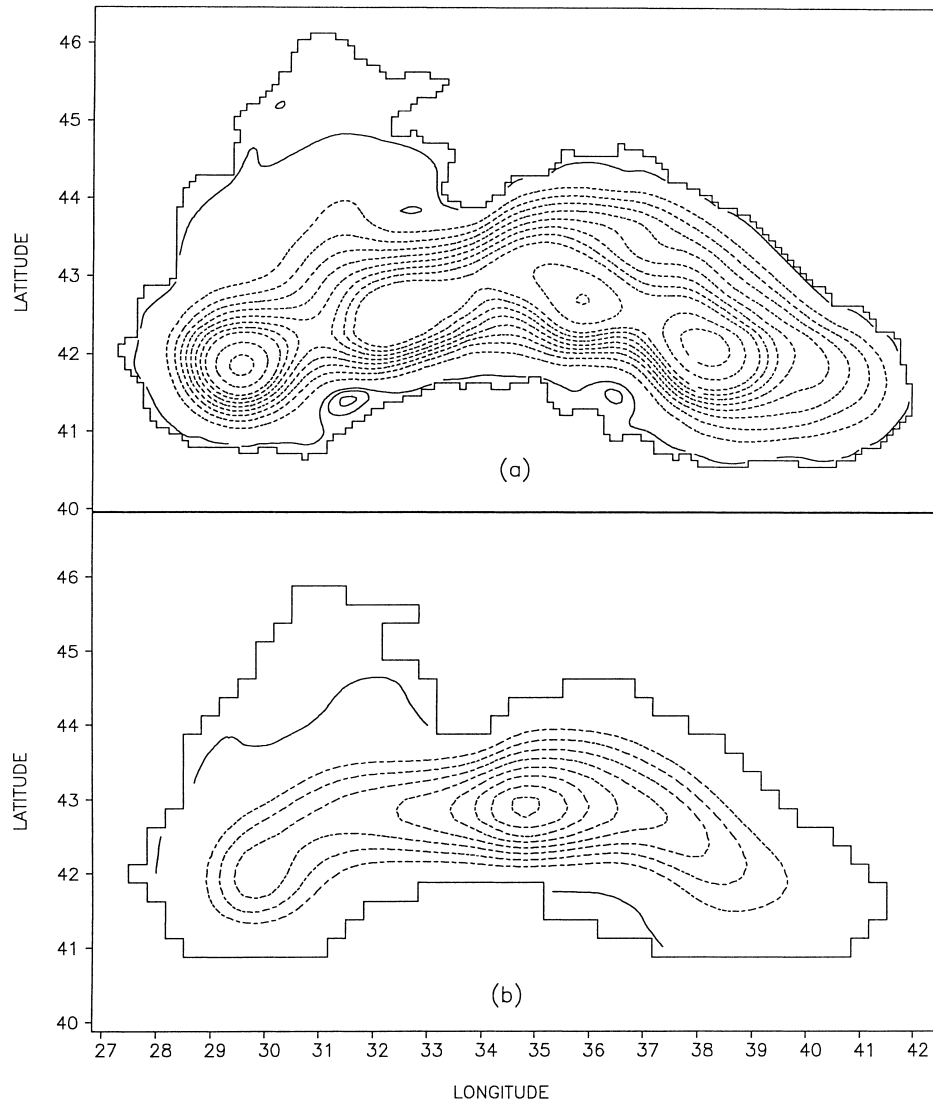


Fig. 2. Annual mean stream function ($CI = 0.5 \text{ Sv}$). To visualize the areas with anticyclonic circulation, the positive values for the stream function are plotted with full lines. The contour interval in these areas is 0.1 Sv . (a) FRM; (b) CRM.

by observations and numerical studies (Filippov, 1968; Blatov et al., 1984; Stanev, 1990; Oguz et al., 1992; Sur et al., 1994). The total transport in the FRM (Fig. 2a) is about two times larger than the one in the CRM (Fig. 2b). A typical feature in the FRM is the existence of anticyclonic eddies between the main gyre and the coast. Though eddy signals tend to cancel in the long term mean, the contours in Fig. 2a plotted with solid lines will reveal the areas where anticyclones are usually observed: along the southern coast and west of Crimea

Peninsula. This result is in a good qualitative agreement with the circulation patterns given in the work of Oguz et al. (1992). As shown by Staneva and Stanev (1997), the vertical circulation associated with these eddies might affect the penetration of the cooled surface water into the deeper layers.

The snapshots of currents in the upper layer demonstrate quasi-repeating patterns with pronounced interannual variability. A strong eddy activity (eddy scales of about 50–200 km) dominates the circulation in the FRM (Fig. 3). Eddies form in the eastern Black Sea and propagate westwards, dissipating along the western coast. This model behavior is a combined effect of basin oscillations and topographic waves (Rachev and Stanev, 1997; Staneva and Stanev, 1997). Such eddy features are not typical in the results of the CRM, where the deviation of the circulation from the mean cyclonic pattern (Fig. 2b) are small and mostly due to the external forces. It is noteworthy that the different circulation in CRM and FRM, associated with quite different vertical motions could affect the SST and the corresponding heat exchange with the atmosphere.

The heat flux parameterization used in the model is based on aerodynamic bulk formulae with stability dependent exchange coefficients (Appendix A). This introduces a non-linear temperature dependence. The ocean response is also non-linear which is mostly due to convection and sub-basin scale motions in FRM. All this in combination could result in different pathways of heat simulated in the FRM and CRM. The differences in the heat flux, when estimated by models with different resolution, are shown in Fig. 4. The annual mean net cooling is -1.7 W m^{-2} in CRM versus -2.08 W m^{-2} in FRM. There are some differences between heat flux patterns in the northwestern part of the sea, where the cooling reaches -80 W m^{-2} in the FRM versus -60 W m^{-2} in the CRM. To support our model simulations, we show in Fig. 4c, the climatic estimates of Golubeva (1991) based on observations. The agreement between the two independent types of data in the areas with extreme cooling (particularly the agreement between climatic data and the results of FRM) is encouraging.

It is noteworthy that the heat flux patterns show a strong decrease of cooling in the FRM along the western coast (between the riverfront and the coast), where the cooling capabilities are reduced due to the extremely strong vertical stability caused by dilution of surface waters. This effect was discovered earlier by Stanev (1990), but the resolution in this study (also in CRM, Fig. 4b) did not allow to resolve sufficiently the coastal frontal area south of the Danube Delta.

The simulations reveal extremely strong variability in the heat flux patterns during the cold part of the year. Severe cooling in some particular days might result in a very large contribution to the total amount of cold water mass formed (this issue is discussed by Stanev et al., 1995). One such event occurred at 28 February 1986 and we will analyze it in more detail in the following. We remind the reader that the upper and lower boundaries of the CIL are usually associated with isotherms 8°C , thus, we see in Fig. 5 that at this particular day there are conditions for local formation of CIW only in the Western Black Sea and in one part of the central region (the solid isolines, temperature 7.8°C or higher, mark approximately the regions where no local formation of CIW is possible). The regions of water mass formation roughly coincide in FRM and CRM.

The snapshots of SST (Fig. 5) indicate one important source of differences between the heat flux estimates in the two models. Though we impose spatially smooth atmospheric forcing (Fig. 5a), strong fronts, meanders, and filaments dominate the SST in the FRM

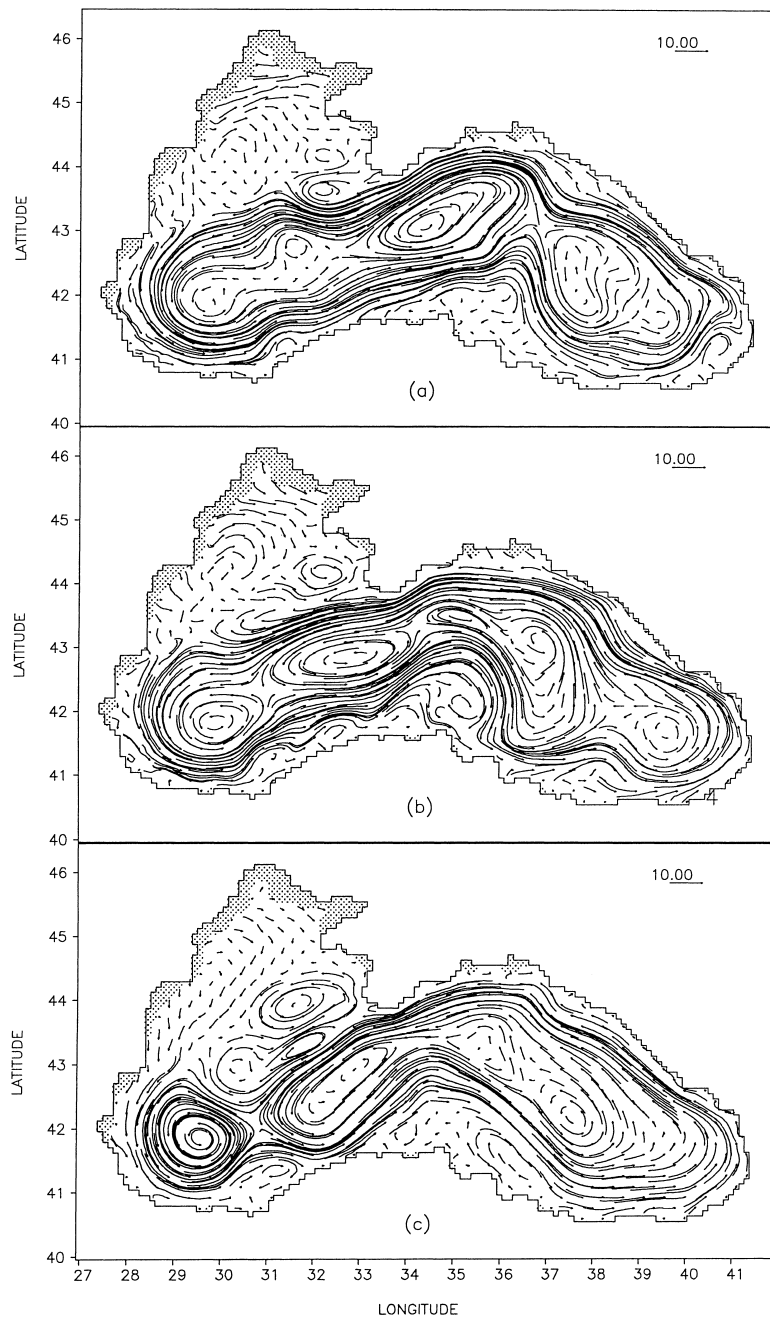


Fig. 3. Snapshots of the horizontal velocity at 20 m. The initial time of the integration coincides with the real time and is 8 January 1979: (a) 22 March 1982, (b) 11 March 1984, (c) 31 March 1986.

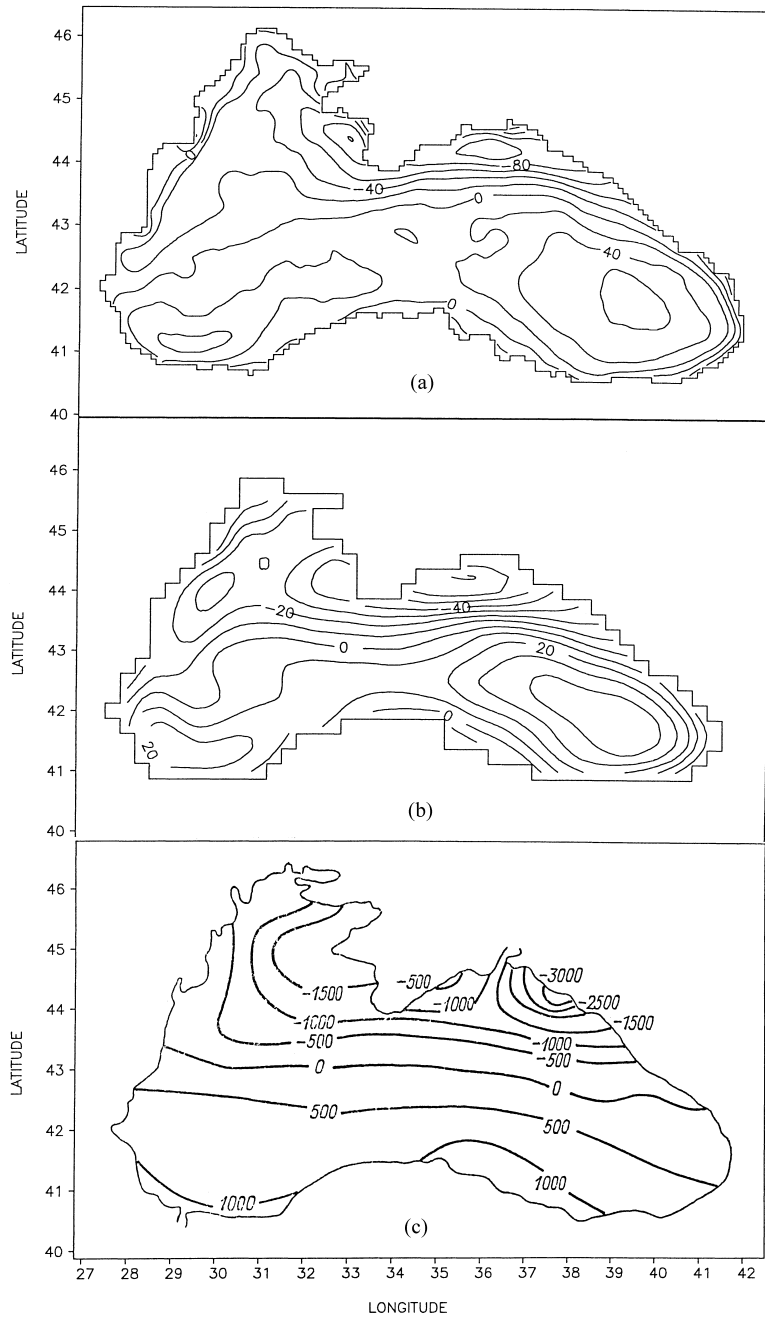


Fig. 4. Annual mean heat flux patterns. (a) FRM (in W m^{-2}), (b) CRM (in W m^{-2}), (c) from Golubeva (1991, Fig. 1. 12, p. 142) (in $\text{MJ m}^{-2}/\text{year}$). To convert the numbers in Fig. 4c in W m^{-2} one has to divide by 32.

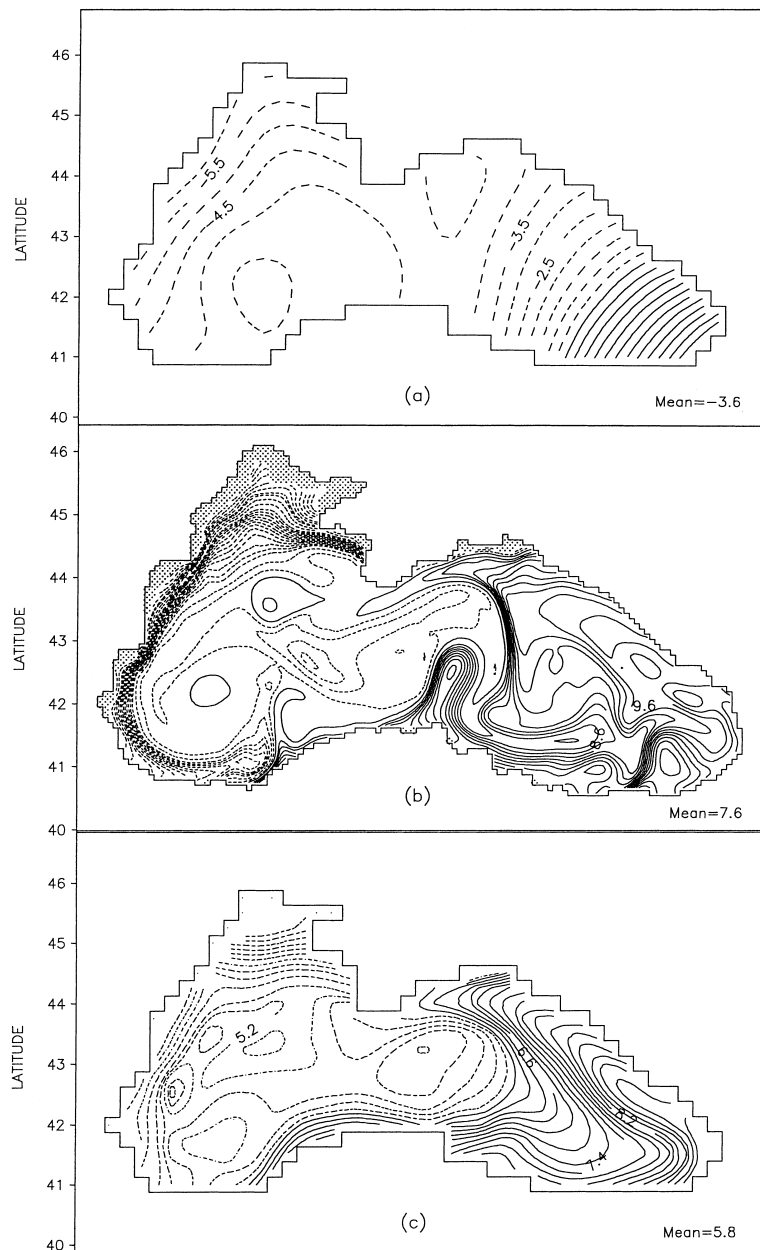


Fig. 5. Snapshots (28 February 1986) of the atmospheric forcing and simulated temperature and salinity at 20 m. To identify positive and negative anomalies, values which are larger than the mean are plotted with full lines. The ones lower than the mean are plotted with dashed lines. (a) Air temperature, CI = 0.5°C , (b) temperature at 20 m, FRM, CI = 0.2°C , (c) temperature at 20 m, CRM, CI = 0.2°C , (d) Sea surface salinity calculated from climatology, CI = 0.2, (e) salinity at 20 m, FRM, CI = 0.1, (f) salinity at 20 m, CRM, CI = 0.1.

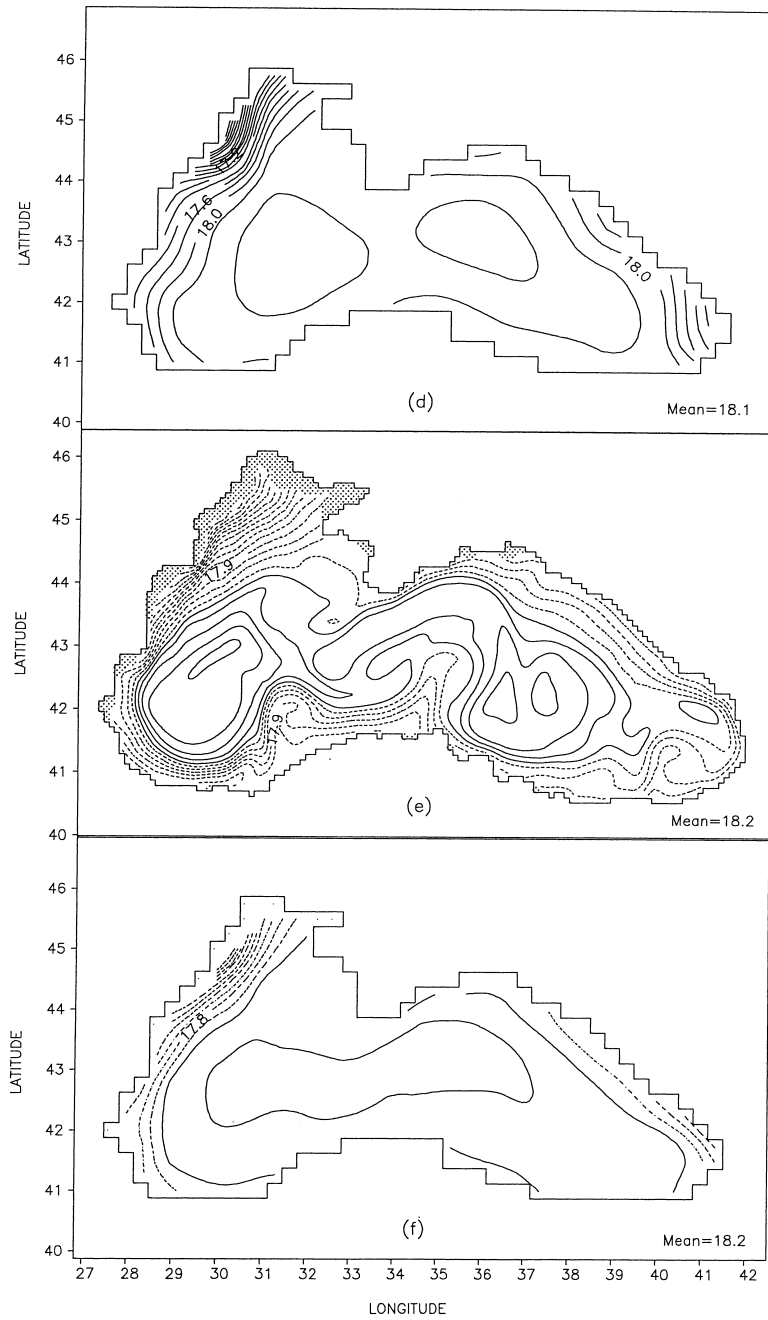


Fig. 5. (Continued).

(Fig. 5b). The isolines in the CRM are much smoother (Fig. 5c). In the western Black Sea, the SST in the coarse resolution model “follows” the air temperature, while in the eastern part the tongue-like shape of isohalines demonstrates that the pattern is affected by the basin circulation (see the transport pattern in this area on Fig. 6). In the FRM (like in the real sea), the SST deviates from the surface forcing over the entire basin. This issue is a key one when estimating heat flux at the sea surface.

The simulations demonstrate that the area of very strong gradients along the western coast (basin temperature minimum of about 2°C) reaches the Sakaria Canyon where a spectacular intrusion of coastal waters into the basin interior is simulated (Fig. 5b). This region is known in the Black Sea oceanography as a region of extreme mixing that results in the termination of the sharp coastal front. Note that not only waters from the up-stream direction are injected into the open sea, but also water east of the canyon that leads to the formation of a pronounced mushroom pattern of temperature. Similar intrusions of coastal

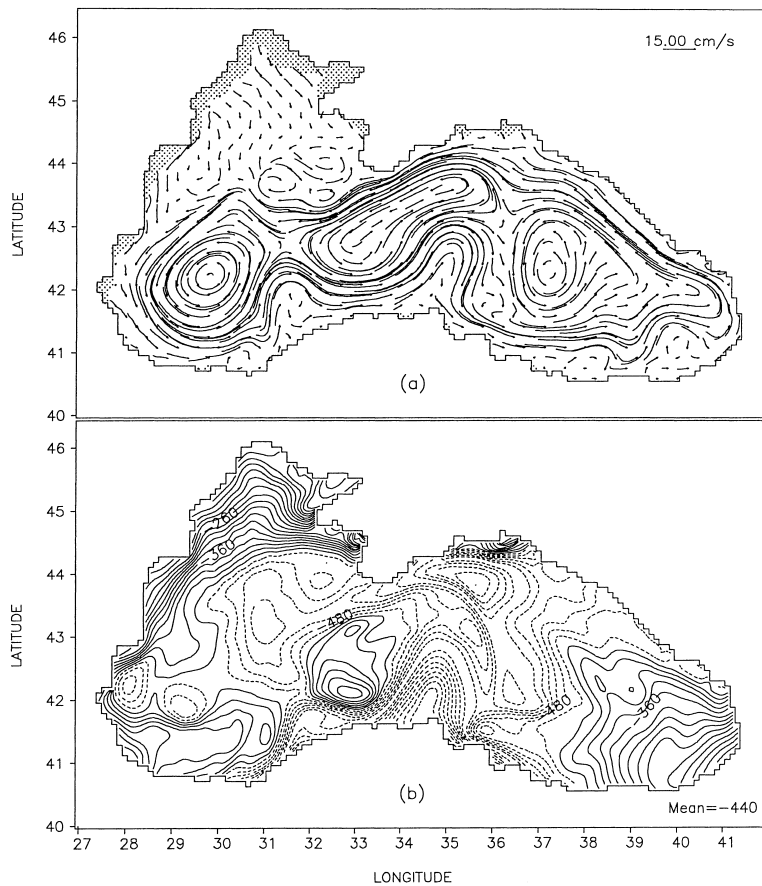


Fig. 6. Horizontal patterns at 28 February 1986. (a) Velocity at 20 m, FRM, (b) sea surface heat flux, FRM, $CI = 20 \text{ W m}^{-2}$, (c) velocity at 20 m, CRM, (d) sea surface heat flux, CRM; $CI = 20 \text{ W m}^{-2}$.

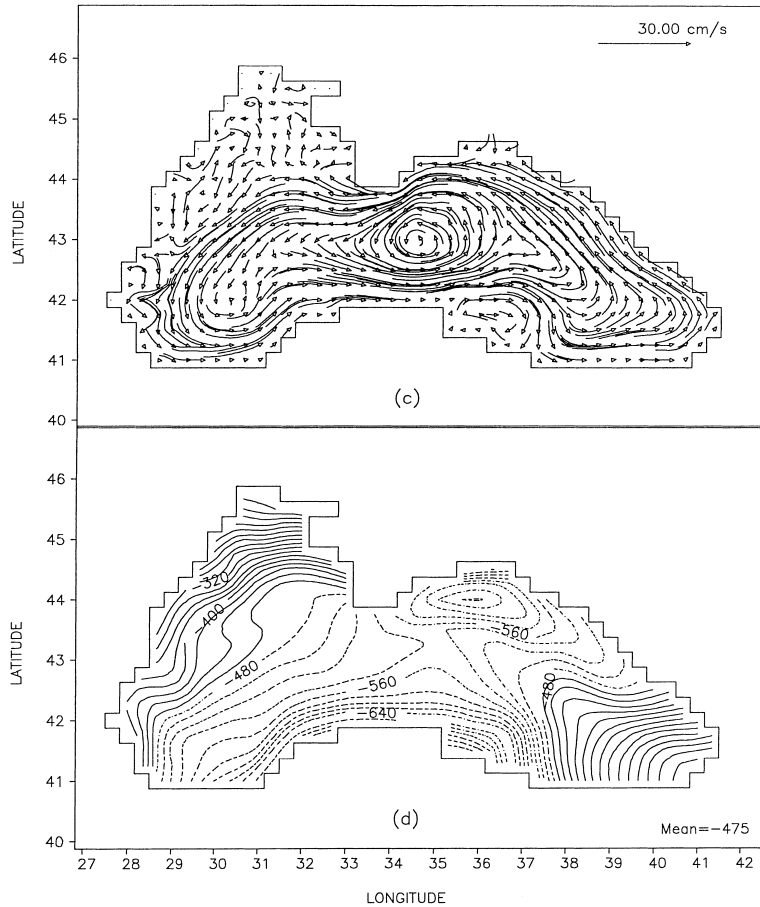


Fig. 6. (Continued).

waters into the open sea have been observed in the satellite data analyzed by Sur et al. (1994). As seen from the comparison with Fig. 5c, these features are missing in CRM simulations. The narrow fronts simulated in the FRM, show how important is to have fine horizontal resolution allowing to resolve the paths of waters formed in the shelf area.

The temperature fields in the deep layers (not shown here) are also dominated by eddy like features, illustrating the response of the pycnocline to propagating eddies. However, due to the very homogeneous vertical stratification of temperature, the horizontal gradients are very small. The maximum difference at 450 m reaches about 0.1°C for the whole sea which compares well with the recent surveys (Aubrey et al., 1991).

The salinity pattern at 17.5 m (Fig. 5e) also proves that the model dynamics dominates salinity in the surface layer (no filaments or meander-like features are observed in the climatological forcing data, Fig. 5d). It is noteworthy that the model periodically generates anticyclonic circulation in the area, where the Batumi eddy is usually observed (see the

patterns plotted with dashed lines in the easternmost Black Sea). This circulation feature is not simulated in the CRM. The horizontal gradients of salinity in the shelf area decrease rapidly with increasing depth, and the isolines tend to follow the continental slope. At deeper layers salinity is very homogenous, which is in agreement with the observations (maximum contrast for the whole basin at 450 m reaches about 0.2).

It follows from the above results that the preconditioning for convection has not only regional dependency (very low temperatures on the north-western shelf), but might depend on pronounced eddies and meanders in the FRM.

Number of studies (e.g. Esbensen and Reynolds, 1981) suggest that the correlation between air temperature and SST is substantially smaller than the product of their mean values. Other studies (Gulev, 1994) do not support this idea. As shown by Staneva et al. (1995) any computation, in which the SST simply follows the atmospheric temperature with constant ΔT , misses the important contribution of the correlation between exchange coefficient C_h and ΔT (see Eq. (A.1)). The poor estimates in such case are due to the lack of time or space correlation between the atmosphere and ocean data. This correlation depends on the horizontal circulation and the feedback between atmosphere and ocean. While the large scale SST might «follow» to some extent the atmospheric temperature, substantial differences exist between the SST and air temperature on smaller scales (compare Fig. 5a and b). The corresponding correlation could have important contribution to the ocean-atmospheric heat exchange.

We analyze below the individual contribution of the correlation terms between wind magnitude V_a , the difference between air and sea surface temperature ΔT , and the exchange coefficient C_h , which enters in the formula for heat flux (Eq. (A.1)). To illustrate their impact on the net heat flux we will analyze the basin mean values. For brevity we do not show the analogous correlation between relative humidity and the rest of the variables.

We display the results in Table 1 in a similar form as in the study of Esbensen and Reynolds (1981). They correspond to the following three SST fields: (1) computed by the CRM, (2) computed by the FRM, (3) computed by the FRM, but smoothed over the neighboring nine grid points. The last is practically a diagnostics on the contribution of

Table 1

Terms in the Reynolds averaged bulk aerodynamic equations for the temperature flux ($10^{-3} \text{ m s}^{-1} \text{ K}$)^a

		$\Delta T = T_w - T_a$	V_a	$C_h V_a \Delta T$	$C_h V_a \Delta T$	$C_h V_a' \Delta T'$	$V_a C_h' \Delta T'$	$C_h' V_a' \Delta T'$	$C_h' V_a' \Delta T'$
January	CRM	1.43	6.070	16.020	14.760	-0.199	0.854	0.661	0.006
	FRM ^b	1.72	6.323	22.944	16.412	0.601	3.967	1.962	0.002
	FRM ^c	1.78	6.113	23.913	18.717	0.771	1.643	2.778	0.002
	FRM ^d	1.79	6.113	23.753	18.720	0.770	2.807	1.454	0.002
April	CRM	-0.47	4.375	0.114	-2.529	0.112	1.971	0.643	-0.053
	FRM ^b	-0.42	4.437	1.571	-2.125	0.224	2.786	0.886	-0.201
	FRM ^c	-0.21	4.337	0.680	-0.704	0.208	1.048	0.160	-0.032
	FRM ^d	-0.13	4.337	2.313	-0.505	0.252	2.351	0.321	-0.109

^a Transfer coefficient of Hellerman and Rosenstein (1983) have been used; SST is as produced in the model.

^b The Entire Sea — all grid points are used for averaging; SST is as produced in the model.

^c The Open Sea — no coast points are used for averaging; SST is as produced in the model.

^d The Open Sea — no coast points are used for averaging; SST is filtered.

the smallest scales in the heat flux estimates. This has been done in order to show the possible difference between the case when “true” data are used and when the estimates are based on smoothed data. Since the results show strong temporal variability, induced by the variability in the atmospheric data, we show averaged estimates for two months: January and April. These months correspond to the periods when the temperature difference between atmosphere and ocean is large (January) and when it is small (April). Due to this difference, the product in the second column is much larger in January than in April.

One conclusion is evident from Table 1, i.e. the cooling in January simulated in the CRM (column 3) is about 20% smaller than in the FRM. In April, when the difference between the atmospheric and sea surface temperatures is small, the estimates in the CRM are about 15 times lower than in the FRM. This result proves that under the same physical parameterizations and forcing the heat flux between atmosphere and ocean can be strongly biased if the horizontal resolution is not properly chosen.

The second conclusion, following from the table is that the contribution of the correlation structures of the fields in January is relatively small in the two models compared to the contribution of the mean fields (column 4). On the contrary, the correlation becomes dominant in April (column 6) causing changes of the sign of sensible heat flux (column 3), compared to the term due to the mean values (column 4).

Smoothing the SST by nine-point filter necessitates excluding some coastal points when comparing the results. Therefore, the third line for each month gives the same estimates as the second one, but with no contribution of coastal points. The comparison between the second and the third lines in January shows that eliminating coastal points increases the rate of cooling. As we showed above (Fig. 5b), the temperature in the coastal zone in the FRM is very low, approaching the air temperature. This tends to reduce the sensible heat (Fig. 4a) in the coastal area. On the contrary, in April, excluding coastal points in the FRM reduces the effect of cooling. More important, here, is to note that smoothing the SST tends to compensate for the role of the predominant correlation in January (compare columns 5 and 6). This is not exactly the case in April, when the estimates based on smoothed SST are several times larger than the standard estimates. This is consistent with the similar results of Gulev (1994) but does not support the ones of Esbensen and Reynolds (1981).

A relevant question to the above analysis is what would be the sensitivity of the model response to increasing horizontal resolution in the atmospheric data. This is an appropriate question, taking into consideration the insufficient resolution of the atmospheric analysis data. A comment on this issue in the context of Black Sea atmosphere-ocean exchange was given by Staneva et al. (1995). The present results demonstrate that the ocean eddies and fronts have much smaller scales than the resolution provided by the atmospheric analysis data (compare Fig. 5a and b). It follows then that there is a strong argument to advocate for better resolution of the atmospheric data. In the present study (a first attempt to address the impact of ocean eddies on the water mass formation in the Black Sea), we decided to elucidate the response of the ocean model to the model resolution only. As will be seen from the results in the remainder of the paper, the impact of ocean eddies is clearly illustrated also under the assumption that the atmospheric forcing data are identical in the two models.

4. Heat exchange with the atmosphere

For the same time when the patterns in Fig. 5 are shown, the cooling in the northern Black Sea reaches local maximum (more than 600 W m^{-2}) in a small area east of Crimea Peninsula (Fig. 6b and d). This extreme cooling is partially due to the advection of relatively warm water from the eastern part of the basin (Fig. 6a and c), increasing the contrast between the atmospheric and sea surface temperature. It is also maintained in the FRM by the downwelling in the area of the local anticyclonic meander, increasing the thickness of the ventilated layer. As proved from the analysis of model simulations (Staneva and Stanev, 1997) and observations (Golubeva, 1991) this is the area of extremely deep penetration of winter cooling.

The impact of synoptic eddies and meanders on the heat exchange is illustrated by the correlation between SST patterns (Fig. 5b) and heat flux patterns (Fig. 6b). This correlation is well pronounced in the area of anticyclonic meander north of Cape Sinop, where the absolute basin wide maximum of cooling for this moment tends to 700 W m^{-2} (the basin mean value during this day is 440 W m^{-2}). Though the lowest temperatures are simulated in the shelf area the cooling is not strong there. This is explained by the small difference between the SST and air temperature, due to the very low heat capacity of shelf water. The later is caused by: (1) the shallow bottom, (2) the large extension of the shelf, reducing the efficiency of exchange with open ocean water, (3) the large dilution, making the stratification in a very thin surface layer an obstacle for convection.

We analyze below the convective heat flux defined as

$$Q^{CF} = \frac{\rho C_p (T_a - T_b)}{\Delta t} \quad (3)$$

where $C_p = 4.12 \cdot 10^3 \text{ J (K kg)}^{-1}$ is the specific heat capacity, ρ the density of the water, T_b and T_a the temperature before and after the convective adjustment at every time step. The snapshot of convective heat flux for the same moment (Fig. 7a) is dominated by number of small-scale features. This is the model surrogate of convective chimneys (we have to keep in mind that they are hydrostatic features in the model). The convection occurs in the model as single bursts of instability formed at sea surface. Some of the model “convective chimneys” are located close to the shelf break, but many are simulated in the area of the anticyclonic meander north of Sinop. Similar features are simulated in the CRM (Fig. 7b), as well, but they are much larger due to the coarse resolution of the model.

If we average the model results in time (one day), the heat flux due to convection shows much smoother patterns which are very different in FRM and CRM (Fig. 7c and d). One well pronounced feature in the convective heat flux simulated in FRM is that it coincides approximately with the periphery of the anticyclonic meander (Fig. 6a). Another peculiarity is the low correlation during this particular day between heat flux at sea surface (Fig. 7e and f) and the ocean convection. This illustrates that the model convection is associated with very strongly pronounced dynamical features (the fringe of the anticyclonic meanders) and makes possible to conclude that the water mass formation is governed by synoptic and sub-basin scale circulation processes.

There are no indications of deep convection in the cyclonic eddies below 55 m (the convection depth is $<40\text{--}50$ m in these areas). However, this does not mean that the convection

in the open sea is negligible for the ventilation of the pycnocline. On the contrary, due to the upwelling in the zones of cyclonic eddies, the isopycnal surfaces outcrop, or approach sea surface, and are directly affected by the atmospheric cooling. This mechanism of water mass formation in the Black Sea was found by Ovchinnikov and Popov (1987) and was later replicated in the numerical simulations of Staneva and Stanev (1997).

We do not extend the above diagnostics towards quantification of the individual contribution of advection and diapycnal mixing to the penetration of cold water into the halocline. This could be easily done, however, the problem is that the mixing/diffusion parameterizations used here are quite simple that precludes quantification of the effects of advection and diapycnal mixing. This statement is well established for the low-resolution models. In the present one, the resolution (better than 10 km) might capture some baroclinic processes associated with the penetration of surface waters into the halocline, thus, increasing the credibility of simulations. However, further studies with either more elaborated mixing parameterizations (Gent and McWilliams, 1990; Griffies et al., 1998) or models in isopycnal coordinates are needed to check the model consequences of using different parameterizations and provide reliable estimates on the contribution of eddies to the ventilation of pycnocline. The studies of Danabasoglu and McWilliams (1995) and Visbeck et al. (1997) give some encouraging examples in this direction. Nevertheless, even in the models in isopycnal coordinates, lots of problems appear that are related to the treatment of diapycnal exchange (McDougall and Dewar, 1998). Thus, we admit that our model representation of water-mass formation might be, to some extent, compromised by the nature in which the horizontal exchange is parameterized. This motivates us to focus, here, only on the local cooling (due to convection). Its regional dependency roughly reveals the role played by the local dynamics.

The difference between local heat exchange and the convective heat flux gives an idea about the efficiency of cooling. The latter is exemplified by two quite different regimes. In the area south of the Kerch Strait the warm surface water advected from the eastern basin maintains the difference between air and sea surface temperature high which results in large heat exchange. However, this cooling is not sufficient to bring surface water into the halocline. The situation is completely different along the shelf break in the western Black Sea where the southward advection of cold shelf waters make the ventilation much more efficient. Thus, the differences between atmosphere-ocean heat exchange in these regions reveals the contribution of mixing. This has been shown earlier by Speer and Tzipermann (1992) who demonstrated that mixing in the surface layer could bias estimates of water mass formation based on heat flux data only. As stated by Lascaratos (1993), the amount of water mass produced by the air-sea fluxes can be considered only as an upper bound of the amount that penetrates into the pycnocline.

The model gives indications that the cooling in the shelf zone enhances convective flux over the continental slope. In this zone, reaching to the south the Burgas Bay, monthly mean convective heat flux at 60 m is strongest along the shelf break (the edge of the zone covered by dashed isolines area in Fig. 8a). In this area, the cold water formed on the shelf tends to sink along the slope (almost the entire slope area in the north-western Black Sea, see Fig. 1, reveals large values of convective cooling). The mixing of shelf with open sea water increases the instability over broader area and triggers the convection at the continental slope. Note that the intrusions of cold waters are not uniform over the entire shelf

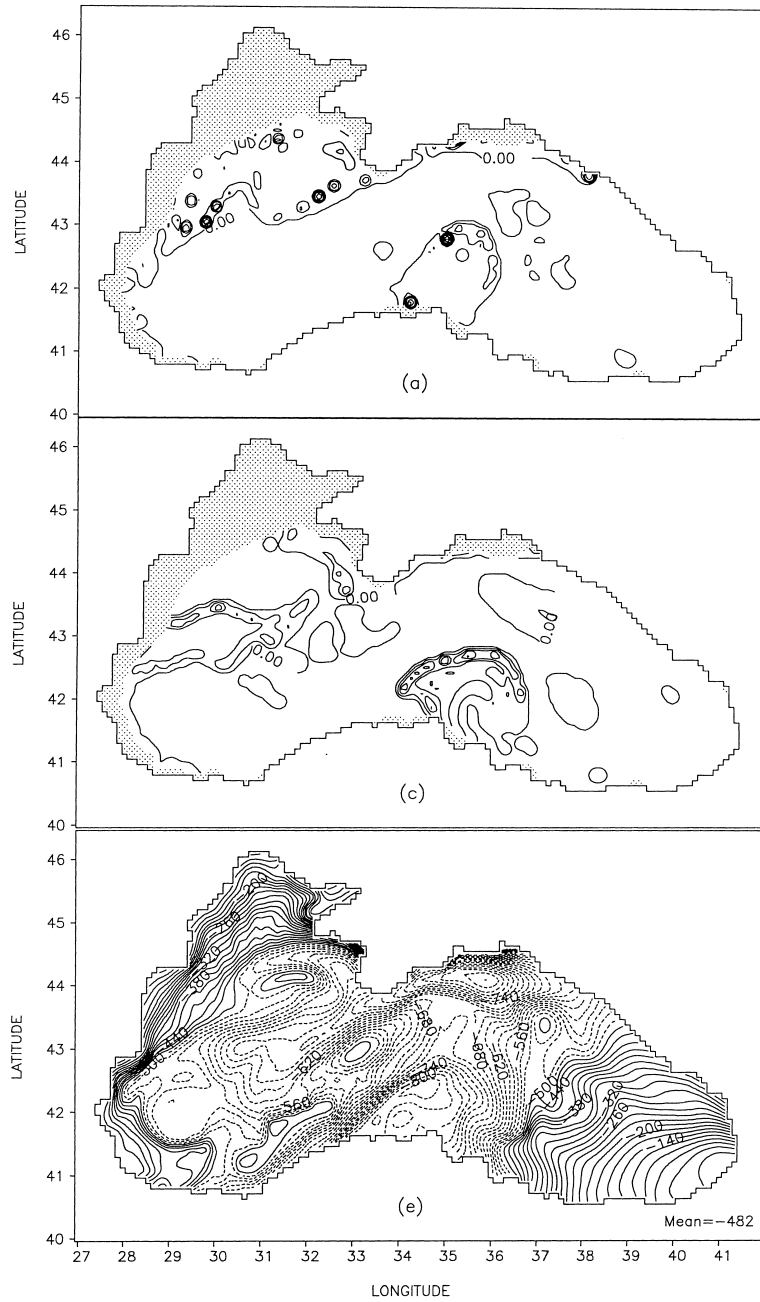


Fig. 7. Horizontal patterns of convective heat flux at 55 m at 28 February 1986, $CI = 20 \text{ W m}^{-2}$. (a) Snapshot in FRM, (b) snapshot in CRM, (c) daily mean in FRM, (d) daily mean in CRM, (e) heat flux at sea surface, FRM, (f) heat flux at sea surface, CRM. Depth of maximum penetration of intense convection in m, (e), after Gertman (1991).

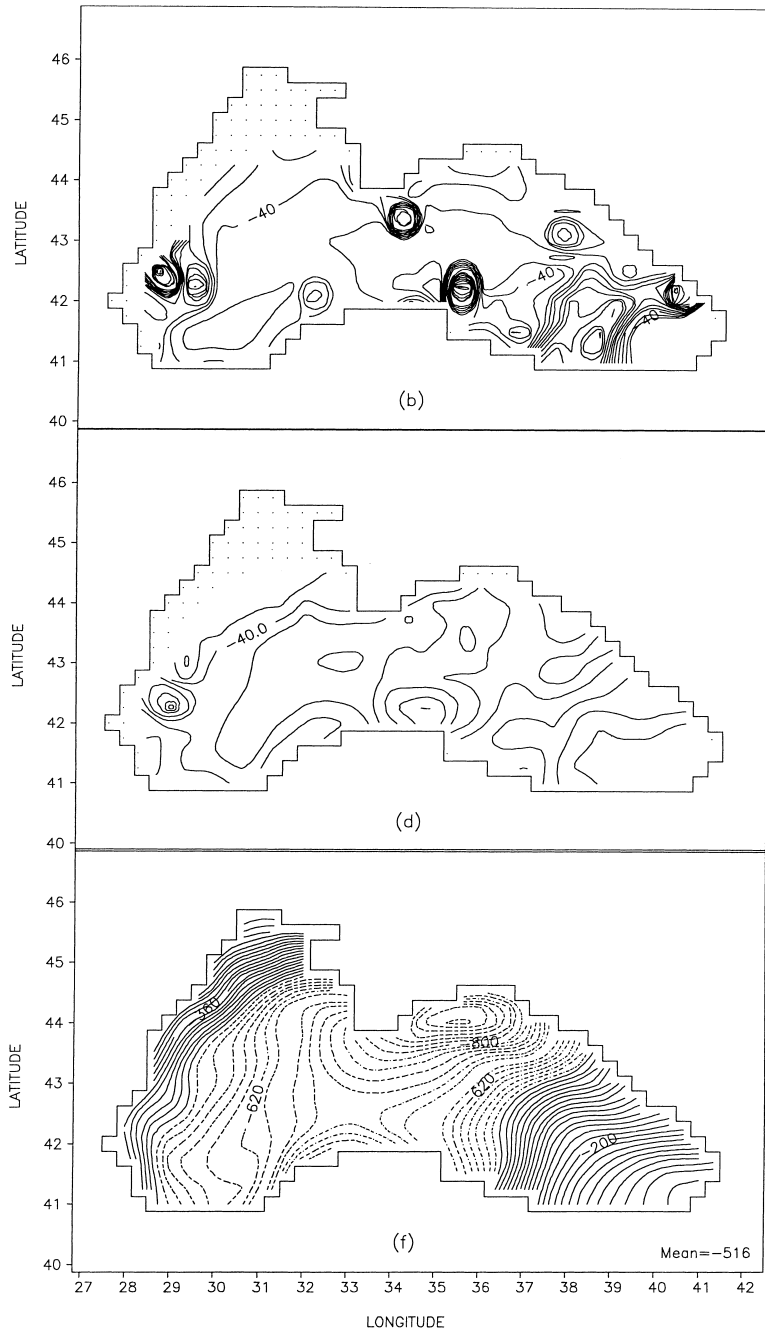


Fig. 7. (Continued).

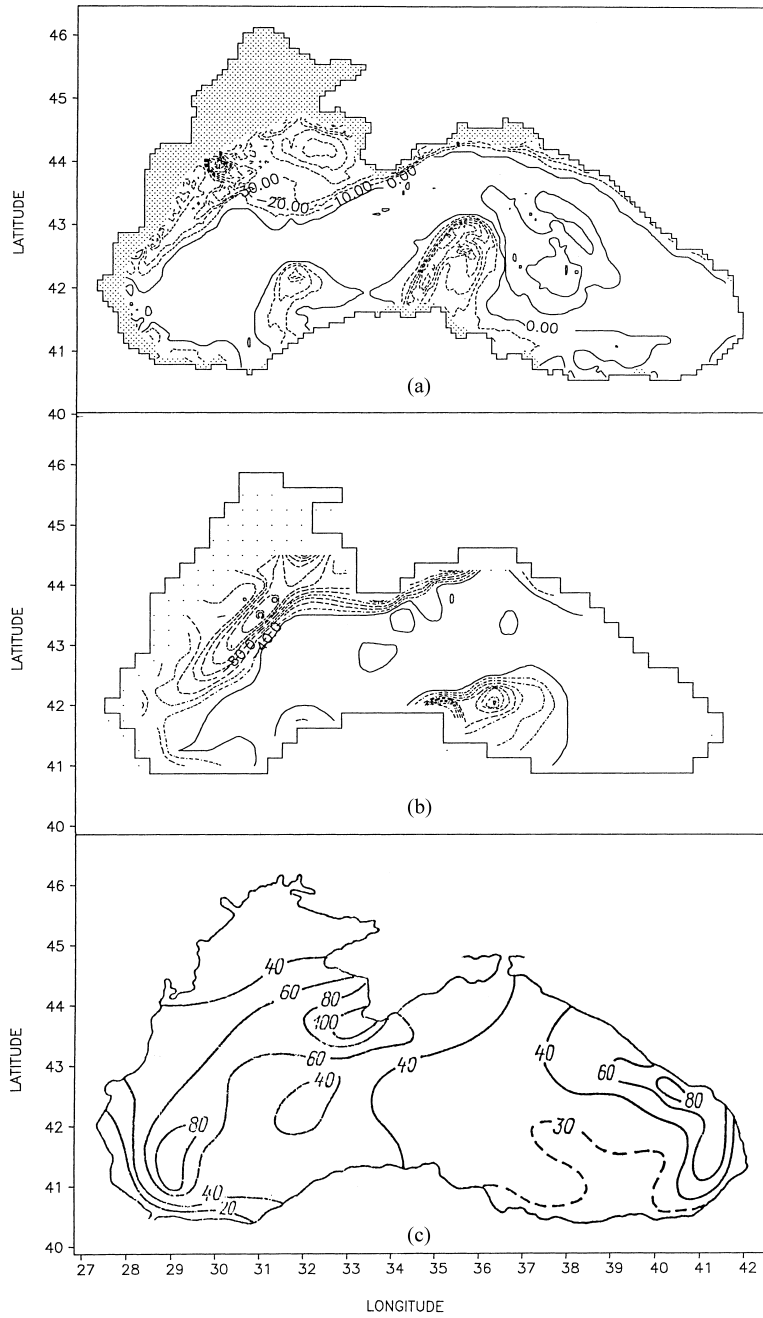


Fig. 8. Monthly mean February convective heat flux at 55 m, $CI = 10 \text{ W m}^{-2}$. Depths shallower than 55 m are shaded. Cooling (negative values) is displayed with dashed lines. (a) FRM, (b) CRM, (c) depth of maximum penetration of intense convection in m (after Gertman, 1991, Fig. 2. 29).

(Fig. 8a), but there are some “preferred” paths. One important difference between the two experiments is noteworthy: the area of maximum convection in the FRM is just at the shelf break, whereas in the CRM this zone is clearly separated from the shelf by an area, where the convective cooling is very small. This supports the result of Staneva and Stanev (1997) showing that the penetration of the cold water into the halocline in this region could only be well resolved in the FRM. The enhanced penetration of CIW into deeper layers over the shelf edge could motivate further interest in the processes associated with the slope convection. Studies in this field with models that better resolve the bottom boundary layer (Beckman and Doscher, 1997; Winton et al., 1998) are needed. This includes also the modeling of frictional bottom boundary layer on a separate two dimensional grid (Pacanowski and Gnanadesikan, 1998) that solves some problems arising from the model representation of topography. The above model developments would make possible to provide more reliable estimates on the role played by the slope convection in the ventilation of halocline.

The downwelling associated with the anticyclonic circulation also affects the penetration of surface waters into the halocline. The convection west of Crimea Peninsula simulated in February is in a good agreement with the horizontal patterns of the maximum penetration depth of convection in the Black Sea (Fig. 8c) based on observations. The annual mean heat flux patterns correlate in this area with the climatic estimates based on survey data, as well (compare with Fig. 4). Increasing the time of averaging to one month (Fig. 8), tends to bring the model estimates for ocean convection in a good consistency with the independent climatic estimates of Gertman (1991) for the region west of Crimea Peninsula, or with the prevailing in this period dynamic features (the two regions of convective cooling associated with the coastal water intrusions) in the region of Sakaria Canyon and Sinop (Figs. 5b and 6a). This means that though the hydrostatic approximation is used in the model, the effects resulting from the model convection look realistic in the FRM. The point, here, is that the inclusion of mesoscale processes increases the physical resolution (geostrophic eddies are diabatic transferring agents, Marshall and Schott, 1999) making possible to more accurately represent the ventilation of pycnocline (more detail about the role and parameterization of eddies in primitive equation models are given in the paper by Treguer et al., 1997).

The above qualitative validation of model performance demonstrates that the anticyclonic area acts not only as a pool of cold waters (Ivanov et al., 1997). Neither is the large cooling capacity of this area (large depth reached by ventilation associated with the vertical circulation) that is the most important for the formation of CIW. The latter factor is more important for the transformation of CIW (Staneva and Stanev, 1997). What we find in this study is that the mechanism associated with the intense convection along the rim of anticyclonic meanders/eddies appears to be significant for cold water mass formation and, what has to be stressed, here, is that this mechanism could be studied under eddy resolution only.

Another important conclusion follows from the comparison of Fig. 8a and b. Unlike the snapshots and the daily mean estimates, the monthly mean convective flux at 55 m shows less different horizontal patterns in both models demonstrating that the climatic characteristics of ocean-atmospheric exchange tend to converge with increasing the time of averaging. In this context, refer to the study of Gulev (1994) demonstrating that at some particular time and space scales the effects of spatial averaging (roughly speaking CRM simulations) and temporal averaging (monthly mean estimates from FRM) might lead to comparable results.

5. Discussion and conclusions

We showed in this paper that the SST in the FRM is dominated by fronts, meanders, and filaments, and deviates strongly from the atmospheric temperature. This is not exactly the case in the CRM where the isolines are smoother. These results are relevant to the fundamental oceanographic issue about how close the SST “follows” the air temperature (Esbensen and Reynolds, 1981; Gulev, 1994). We demonstrated that large and area dependent differences could exist between the SST and air temperature, creating an important eddy-dominated component of the ocean-atmospheric heat exchange. The CIW formation depends on number of small-scale features. Among them we identify: (1) short period, single bursts of instability in the vicinity of the continental slope; (2) anticyclonic eddies between the main gyre and the coast enhancing the downwelling and giving a net contribution to the pumping of cold water into the CIL just on the fringe (not over the whole area dominated by anticyclonic circulation). These elements of the circulation are not sufficiently resolved in the CRM.

We showed that the total annual mean mass transport in the FRM is about two times larger than the one in the CRM (Fig. 2). Could this large difference have a pronounced impact on the CIW formation, or a compensation between eddy and mean transport occurs (as in some ocean models Cox, 1985; Bryan, 1986)? To facilitate the answer to this question, we remind the reader that the vertical circulation in the Black Sea is much weaker than the horizontal one and large changes in the horizontal circulation are not accompanied by large (in absolute values) changes in the vertical circulation (Stanev, 1990; Rachev and Stanev, 1997). Thus, the intensification of the circulation does not automatically result in a pronounced vertical overturning with a clear impact on the water mass formation. This gives one possible explanation why the net heating/cooling is not too different in the two models.

To make our discussion more conclusive, we will summarize below some quantitative results. The comparison between the net heat exchange with the atmosphere in 1986 simulated with different horizontal resolution (-1.7 W m^{-2} in the CRM versus -2.08 W m^{-2} in the FRM) indicates that: (1) The contribution of the increased resolution in the net cooling at the sea surface is $<20\%$. (2) The difference in the net buoyancy flux is very small number compared to the local/instantaneous values, reaching hundreds of W m^{-2} . We remind that these differences in the heat flux estimates of the two models are caused only by the differences in the model resolution, but not in the atmospheric data.

The response of the water masses to changing horizontal resolution is illustrated in Fig. 9, where the basin averaged temperature in the CIL (55 and 75 m) is shown for the two experiments. The increased horizontal resolution in FRM results in stronger cooling that is partially compensated by the stronger heating in fall. The amplitude of the seasonal variations is smaller in the CRM, and the two simulations give almost identical values in the beginning of the next year. This result shows that the contribution of eddies might be negligible for the annual averaged characteristics of water masses. However, the seasonal variability in the CIL is very sensitive to the eddy contribution in the heat exchange with the atmosphere. We could then conclude that eddies give not only a mechanism for penetration of heat into the ocean, but also tend to substantially change its distribution.

The seasonal variability shows different behavior only 20 m deeper (at 75 m), where the model thermodynamics is not strongly affected by direct atmospheric cooling (remind that the processes in the Black Sea are decoupled in the vertical by the strong stratification). The cold water content at this depth is maintained rather by dynamics and mixing with the waters from above. Thus, a time lag between temperature minima at the two depths is observed (the basin wide minimum at 75 m is reached in June–July, when sufficient quantity of CIW are transported into the basin interior from the shelf-beak area). The simulated CIL in FRM shows lower minimum temperatures than in CRM, which demonstrates that by increasing the eddy activity along the rim current (that is also the usual situation in the real basin), the rate of ventilation of coastal zone increases. This has far reaching consequences. By exchanging waters between the coastal and open sea areas (often diapycnally), the model tends to modify the vertical stratification. It is clearly seen in Fig. 9a and b that the vertical temperature gradient is smaller in the end of winter and larger by the end of fall in the fine resolution model. We remind, here, that the parameterizations in the vertical are the same in the two models. Thus, we can conclude that the formation (and not only the storage) of CIW depends on mesoscale processes.

It follows from the above results that the impact of eddy variability on the CIW formation is one part of the more general issue being to what extent the interaction between atmosphere and ocean in the region of the Black Sea is dominated by eddies. The lack of feedback mechanisms in our model could bias the heat flux calculations, even in case of using perfect ocean model. We can expect, thus, that in a coupled atmosphere-Black Sea model the air-sea heat flux anomalies will reduce in comparison to the present estimations, therefore, the conclusions given above could be regarded as preliminary ones. Further analysis aiming to better understand the specific role of the Black Sea eddies and sub-basin scale circulation for the heat transport between the ocean and atmosphere are needed, in which the atmosphere has to be active, that is it has to adjust to the heat exchange (Rahmsdorf and Willebrand, 1995; Xu et al., 1995).

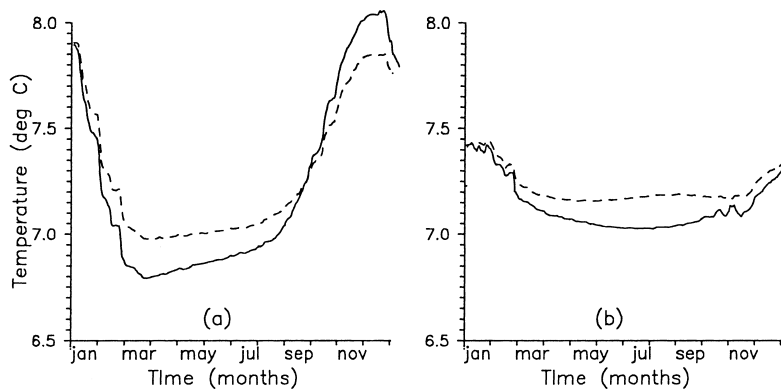


Fig. 9. Time series of basin-averaged temperature, FRM (full line) and CRM (dashed line): (a) at 55 m; (b) at 75 m.

Acknowledgements

We thank J. M. Beckers and the anonymous reviewer for number of constructive suggestions that helped us in improving the paper. This work is supported by the contract with the CEC No. ERBCIPDCT930016.

Appendix A. Parameterizations of the surface forcing

The net heat flux at sea surface can be represented as: $Q^T = Q_s - Q_u$, where Q_s is the downward flux of solar radiation and Q_u the net upward flux of radiation emitted by the sea surface via radiative and evaporative–conductive processes. The net upward flux $Q_u = H_a + LE_a + Q_b$ includes the net flux of long wave radiation loss Q_b , sensible H_a and latent LE_a heat flux ($L = 2.501.106 \text{ J kg}^{-1}$ is the latent heat of vaporization). For the long wave radiation loss we use the formulae of Berliand and Berliand (1952), modified as in Rosati and Miyakoda (1988), and for the sensible and latent heat flux, the following bulk formulae:

$$H_a = \rho_a C_p C_h |W| \times (T_s - T_a) \quad (\text{A.1})$$

$$E_a = \rho_a C_e |W| \times [e_{\text{sat}}(T_s) - re_{\text{sat}}(T_a)] \frac{0.622}{p_a} \quad (\text{A.2})$$

where T_s and T_a are the SST and the atmospheric temperature at 1000 mbar, respectively, $e_{\text{sat}}(T_a)$ polynomial approximation (Lowe, 1977), ρ_a the density of the air, p_a the surface air pressure ($p_a = 1013 \text{ mbar}$), $|W|$ the surface wind magnitude, C_p the specific heat capacity ($C_p = 1.005 \times 10^3 \text{ J (kg K)}^{-1}$), C_h , C_e are turbulent exchange coefficients.

Wind stress is parameterized as

$$(\tau^\lambda, \tau^\varphi) = \rho_a C_d |W| (W_x, W_y) \quad (\text{A.3})$$

where W_x , W_y are the wind components, C_d the drag coefficient. Turbulent exchange and drag coefficients are assumed to be equal and dependent on the difference between atmospheric and sea surface temperature (Hellerman and Rosenstein, 1983, see also Staneva et al., 1995). Momentum and heat fluxes are calculated interactively. The model calendar is set to correspond to the real time of the atmospheric data set, and the atmospheric data are interpolated at every time step. The model time is used to calculate the solar radiation at every grid point. The fractional cloud cover is inferred at each model step from the monthly mean data (Sorkina, 1974). The value of T_s in the parameterizations for the wind stress and for the net upward flux is set to be equal to the current model SST.

Appendix B. Parameterizations of subgrid processes

Mixing and diffusion in the horizontal are parameterized with biharmonic operators. The coefficients are: $A_h = K_h = 0.8 \times 10^{19} \text{ cm}^4 \text{ s}^{-1}$ in the model with coarse resolution and $A_h = K_h = 0.1 \times 10^{19} \text{ cm}^4 \text{ s}^{-1}$ in the fine resolution one (for the model sensitivity to these parameters see Stanev et al., 1997). The vertical mixing coefficient is $A_v = 1.5 \text{ cm}^2 \text{ s}^{-1}$.

The vertical diffusion coefficient K_v is stability dependent,

$$K_v = aN^{-1} \quad (\text{B.1})$$

where N is the Väisälä frequency, $a = 0.004 \text{ cm}^2 \text{ s}^{-2}$, (see also Gargett, 1984 and Lewis and Landing, 1991). In the 30 m surface, K_v decreases linearly from its surface value of $1 \text{ cm}^2 \text{ s}^{-1}$ to its value at 30 m calculated from Eq. (B.1), to take into account (at least very roughly) for the increased diffusion in the mixed layer. Below 30 m, K_v is calculated from Eq. (B.1). Details on the model sensitivity to different parameterizations are given by Stanev et al. (1997).

References

- Aubrey, D.G., Oguz, T., Demirov, E., Ivanov, L., McSherry, T., Diaconu, V., Nikolaenko, E., 1991. Hydroblack '91 CTD Intercalibration Workshop, Woods Hole, USA, 1–10 December 1991, Intergovernmental Oceanographic commission, Workshop Report N91, 56 pp. and 5 Annexes.
- Beckman, A., Doscher, R., 1997. A model for improved representation of dense water spreading over topography in geo-potential coordinate models. *J. Phys. Oceanogr.* 27, 581–591.
- Berliand, M.E., Berliand, T.G., 1952. Measurement of the effective radiation of the Earth with varying cloud amounts. *Iv. Akad. Nauk. SSSR, Ser. Geofiz.*, 1, 64–78 (in Russian).
- Blatov, A.S., Bulgakov, N.P., Ivanov, V.A., Kosarev, A.N., Tujilkin, V.S., 1984. Variability of hydrophysical fields in the Black Sea. *Gidrometeoizdat, Leningrad*, 240 pp. (in Russian).
- Bryan, K., 1969. A numerical method for the study of the circulation of the World Ocean. *J. Comput. Phys.* 3, 347–378.
- Bryan, K., 1986. Poleward buoyancy transport in the ocean and mesoscale eddies. *J. Phys. Oceanogr.* 16, 927–933.
- Cox, M., 1985. An eddy resolving numerical model of the ventilated thermocline. *J. Phys. Oceanogr.* 15, 1312–1324.
- Danabasoglu, G., McWilliams, J.C., 1995. Sensitivity of the global ocean circulation to parameterization of mesoscale tracer transport. *J. Climate* 8, 2967–2980.
- Esbensen, S.K., Reynolds, R.W., 1981. Estimating monthly averaged air-sea transfers of heat and momentum using the bulk aerodynamic method. *J. Phys. Oceanogr.* 11, 457–465.
- Filippov, D.M., 1968. Circulation and Water Composition of the Black Sea, Nauka, Moscow, 136 pp. (in Russian).
- Friedrich, H.J., Stanev E.V., 1988. Parameterization of the vertical diffusion in a numerical model of the Black Sea. In: Nihoul, J.C.J., Jamart, B.M. (Eds.), *Small-Scale Turbulence and Mixing in the Ocean*. Elsevier, Amsterdam, pp. 151–167.
- Gargett, A.E., 1984. Vertical eddy diffusivity in the ocean interior. *J. Mar. Res.* 42, 359–393.
- Gent, P., McWilliams, J., 1990. Isopycnal mixing in ocean circulation models. *J. Phys. Oceanogr.* 20, 150–155.
- Gertman, I., 1991. *Struktura vod moria (composition of sea water)*. In: Simonov, A.I., Altman, E.N. (Eds.), *Hydrometeorology and Hydrochemistry of the USSR Seas, Vol. 4: The Black Sea*. pp. 166–174 (in Russian).
- Golubeva, Z., 1991. Heat balance at sea surface. In: Simonov, A.I., Altman, E.N. (Eds.), *Hydrometeorology and Hydrochemistry of the USSR Seas, Vol. 4: The Black Sea*. pp. 166–174 (in Russian).
- Griffies, S.M., Gnanadesikan, A., Pacanowski, R.C., Larichev, V.C., Dukowicz, J.K., Smith, R.D., 1998. Isonutral diffusion in z-coordinate ocean model. *J. Phys. Oceanogr.* 28, 805–830.
- Gulev, S.K., 1994. Influence of space-time averaging on the ocean-atmosphere exchange estimates in the North Atlantic midlatitudes. *J. Phys. Oceanogr.* 24, 1236–1255.
- Hasselmann, K., 1976. Stochastic climate models. Part I. Theory. *Tellus* 28, 473–485.
- Hellerman, S., Rosenstein, M., 1983. Normal monthly wind stress over the world ocean with error estimates. *J. Phys. Oceanogr.* 13, 1093–1104.
- Ivanov, L.I., Besiktepe, S., Ozsoy, E., 1997. The Black Sea cold intermediate layer. In: Ozsoy, E., Mikaelyan, A. (Eds.), *Sensitivity to Change: Black Sea, Baltic Sea and North Sea*, Kluwer Academic Publishers, Dordrecht, pp. 253–266.
- Klinger, B., Marshall, J., Send, U., 1996. Representation of convective plumes by vertical adjustment. *J. Geophys. Res.* 101 (C8), 18175–18182.

- Lascaratos, A., 1993. Estimation of deep and intermediate water mass formation rates in the Mediterranean Sea. *Deep-Sea Res.* II 40, 1327–1332.
- Large, W.G., Holland, W.R., Evans, J.C., 1991. Quasi-geostrophic ocean response to real wind forcing: the effects of temporal smoothing. *J. Phys. Oceanogr.* 21, 998–1017.
- Lewis, B.L., Landing, W.N., 1991. Manganese and iron in the Black Sea. *Deep-Sea Res.* 38, S773–S805.
- Marotzke, J., 1991. Influence of convective adjustment on the stability of the thermohaline circulation. *J. Phys. Oceanogr.* 21, 903–907.
- Marshall, J., Schott, F., 1999. Open ocean deep convection: observations, models and theory. *Rev. Geophys.* 37 (1), 1–64.
- McDougall, T.J., Dewar, W.K., 1998. Vertical mixing and cabbeling in layered models. *J. Phys. Oceanogr.* 28, 1458–1480.
- Oguz, T., La Violette, P.E., Unluata, U., 1992. The upper layer circulation of the Black Sea: its variability as inferred from hydrographic and satellite observations. *J. Geophys. Res.* 97, 12569–12584.
- Oguz, T., Malanotte-Rizzoli, P., 1996. Seasonal variability of wind and thermohaline-driven circulation in the Black Sea. *J. Geophys. Res.* 101, 16551–16569.
- Ovchinnikov, I.M., Popov, Y.I., 1987. Evolution of the cold intermediate layer in the Black Sea. *Oceanology* 27, 555–560.
- Pacanowski, R.C., Dixon, K., Rosati, A., 1991. The GFDL Modular Ocean Model Users Guide, Version 1.0. GFDL Ocean Group Technical Report, No. 2, 176 pp.
- Pacanowski, R.C., Gnanadesikan, A., 1998. Transient response in a 3-level ocean model with bottom topography resolved using the method of partial cells. *Month. Wea. Rev.* 12, 3248–3270.
- Rahmsdorf, S., Willebrand, J., 1995. The role of temperature feedback in stabilizing the thermohaline circulation. *J. Phys. Oceanogr.* 25, 787–805.
- Rachev, N.H., Stanev, E.V., 1997. Eddy processes in semi-enclosed seas. A case study for the Black Sea. *J. Phys. Oceanogr.* 27, 1581–1601.
- Rosati, A., Miyakoda, K., 1988. A general circulation model for the upper ocean simulation. *J. Phys. Oceanogr.* 18, 1601–1626.
- Sorkina, A.I. (Ed.), 1974. Reference Book on the Black Sea Climate, Moscow, Gydrometeoizdat, 406 pp. (in Russian).
- Speer, K., Tzipermann, E., 1992. Rates of water mass formation in the north Atlantic ocean. *J. Phys. Oceanogr.* 22, 93–104.
- Stanev, E.V., 1988. Numerical study on the Black Sea circulation. *Mitteilungen des Instituts fuer Meereskunde der Universitaet Hamburg, Hamburg, Vol. 28*, 232 pp.
- Stanev, E.V., 1990. On the mechanisms of the Black Sea circulation. *Earth-Sci. Rev.* 28, 285–319.
- Stanev, E.V., Roussenov, V.M., Rachev, N.H., Staneva, J.V., 1995. Sea response to atmospheric variability. Model study for the Black Sea. *J. Mar. Syst.* 6, 241–267.
- Stanev, E.V., Staneva, J.V., Roussenov, V.M., 1997. On the Black Sea water mass formation. Model sensitivity study to atmospheric forcing and parameterization of some physical processes. *J. Mar. Syst.* 13, 245–272.
- Staneva, J.V., Stanev, E.V., 1997. Cold intermediate water formation in the Black Sea. Analysis of numerical model simulations. In: Ozsoy, E., Mikaelyan, A. (Eds.), *Sensitivity to Change: Black Sea, Baltic Sea and North Sea*, NATO Series. Kluwer Academic Publisher, Dordrecht, pp. 375–393.
- Staneva, J.V., Stanev, E.V., 1998. Oceanic response to atmospheric forcing derived from different climatic data sets. intercomparison study for the Black Sea. *Oceanol. Acta* 21, 393–417.
- Staneva, J.V., Stanev, E.V., Rachev, N.H., 1995. Heat balance estimates using atmospheric analyses data: a case study for the Black Sea. *J. Geophys. Res.* 100, 18581–18596.
- Sur, H.I., Ozsoy, E., Unluata, U., 1994. Boundary current instabilities, upwelling, shelf mixing and eutrophication processes in the Black Sea. *Progr. Oceanogr.* 33, 249–302.
- Treguer, A.M., Held, I.M., Larichev, V.D., 1997. On the parameterization of quasigeostrophic eddies in primitive equation ocean models. *J. Phys. Oceanogr.* 27, 567–580.
- Unluata, U., Oguz, T., Latif, M.A., Özsoy, E., 1990. In: Pratt, L.J. (Ed.), *On the Physical Oceanography of the Turkish Straits, the Physical Oceanography of Sea Straits*, NATO/ASI Series, Kluwer Academic Publishers, Dordrecht, pp. 25–60.

- Visbeck, M., Marshall, J., Haine, T., Spell, M., 1997. Specification of eddy transfer coefficients in coarse-resolution ocean circulation models. *J. Phys. Oceanogr.* 27, 381–402.
- Willebrand, J., 1978. Temporal and spatial scales of the wind field over the North Pacific and North Atlantic. *J. Phys. Oceanogr.* 8, 1080–1094.
- Winton, M., Halberg, R., Gnanadesikan, A., 1998. Simulation of density-driven frictional downslope flow in z -coordinate ocean models. *J. Phys. Oceanogr.* 28, 2163–2174.
- Xu, W., Greatbach, R.J., Lin, C.A., 1995. The sensitivity of an eddy-resolving ocean model to the surface thermal boundary conditions. *J. Geophys. Res.* 100 (C8), 15899–15914.